Measurement of Evaporation Residue and Fission Cross Sections of the Reaction ^{30}Si + ^{238}U at Subbarrier Energies

**K. Nishio,*,a S. Hofmann,†,b,c H. Ikezoe,a F. P. Heßberger,b D. Ackermann,b
S. Antalic,d V. F. Comas,e Z. Gan,f S. Heinz,b J. A. Heredia,e J. Khuyagbaatar,b
B. Kindler,b I. Kojouharov,b P. Kuusiniemi,g B. Lommel,b M. Mazzocco,b
S. Mitsuoka,a Y. Nagame,a T. Ohtsuki,h A. G. Popeko,i S. Saro,d H. J. Schött,b
B. Sulignano,b,j A. Svirikhin,i K. Tsukada,a K. Tsuruta,a and A. V. Yeremini**

a*Japan Atomic Energy Agency, Tokai, Ibaraki 319-1195, Japan*
b*Gesellschaft für Schwerionenforschung mbH, D-64220 Darmstadt, Germany*
c*Institut für Kernphysik, Johann Wolfgang Goethe-Universität, D-60486 Frankfurt am Main,Germany*
d*Department of Nuclear Physics, Comenius University, SK-84215 Bratislava, Slovakia*
e*Higher Institute of Technologies and Applied Sciences, Habana 10400, Cuba*
f*Institute of Modern Physics, Chinese Academy of Sciences, Lanzhou 730000, China*
g*CUPP, University of Oulu, FIN-86801 Pyhäjärvi, Finland*
h*Laboratory of Nuclear Science, Tohoku University, Sendai 982-0826, Japan*
i*Flerov Laboratory of Nuclear Reactions, JINR, 141 980 Dubna, Russia*
j*Institut für Kernchemie, Johannes Gutenberg-Universität Mainz, D-55099 Mainz, Germany*

Effects of the prolate deformation of ^{238}U on fusion were studied in the reaction ^{30}Si + ^{238}U at bombarding energies close to the Coulomb barrier. The fission (capture) cross sections were measured at the JAEA tandem accelerator to see the enhancement of the cross sections in the subbarrier energy due to the lower Coulomb barrier in the collisions of projectile at the polar sides of ^{238}U. In order to obtain the direct evidence for complete fusion, evaporation residue cross sections were measured at UNILAC of GSI. At the subbarrier energy of $E_{c.m.} = 133.0$ MeV, where only polar collisions to ^{238}U occur, we measured three spontaneously fissioning nuclei which we assigned to the isotope ^{264}Sg. The obtained cross section (10^{+10}_{-6}) pb was smaller than the calculation that the system captured at the polar collisions results in complete fusion, suggesting the competition between fusion and quasifission. At the above barrier energy of $E_{c.m.} = 144.0$ MeV, where collisions on the equatorial side of ^{238}U start to contribute, we observed α-decay chains starting from ^{263}Sg and the cross section was determined to be (67^{+67}_{-37}) pb. The data was reproduced by the calculation that the system captured from the equatorial side of ^{238}U results in complete fusion.

1. Introduction

Two types of fusion reactions were successfully used in synthesis of heavy and superheavy elements (SHE). These are the cold fusion reactions based on lead or bismuth targets and the hot fusion reactions based on actinide targets. Using cold fusion reactions isotopes of elements up to proton number 112 (Reference 1) were produced at GSI in Darmstadt, Germany, up to proton number 113 (Reference 2) at RIKEN in Wako, Japan. Hot fusion reactions were used to produce isotopes of elements up to 116 and one isotope of element 118 (References 3 and 4) were produced at FLNR in Dubna, Russia.

Another difference between two reactions is associated with the static deformation of the target nuclei. Experimental data for excitation functions producing SHEs reveal that in the case of cold fusion the highest cross sections are obtained at beam energies where a contact configuration between projectile and spherical target nucleus is just reached.[1] In the hot fusion the cross-section maxima were measured at beam energies which are high enough so that projectile (^{48}Ca) and prolate target nuclei can come into contact at minimal distance (equatorial collisions) and thus form a most compact starting configuration on the way to the compound nucleus. The cross sections drop rapidly when the energy is decreased to values where the inter-

action is limited to polar collisions. In this case the probability for re-separation of the reaction partners is high.

However, the results are different for significantly lighter projectiles than ^{48}Ca. In the reaction ^{16}O + ^{238}U, the experimental data show a large enhancement of evaporation residue (ER) cross sections at subbarrier energies,[5] compared to the calculation based on the one dimensional barrier penetration model in the fusion process, and the system which overcomes the Coulomb barrier results in complete fusion also for subbarrier energies. The fusion probability is thus expected to be sensitive to the projectile mass (charge) for the polar collisions, whereas fusion would be less sensitive to projectile mass for equatorial collisions.

In order to study the anticipated phenomena, it is needed to make a systematic measurement by changing projectiles. Here, we report on the results for the reaction ^{30}Si +^{238}U,[6] where the projectile is right in the middle between ^{16}O and ^{48}Ca.

Firstly, we measured the fission cross sections for this reaction, which represents the probability of the system captured inside the Coulomb barrier. The cross sections were largely influenced by the properties of the colliding nuclei, especially prolate deformation of ^{238}U. Secondly, we have produced the evaporation residues (ER) as the direct evidence of complete fusion, and their cross sections were compared with calculations from fusion evaporation models taking into account the effects of the prolate deformation of ^{238}U on fusion. Similar arguments were discussed and presented in earlier works on reactions using prolately deformed target nuclei of rare-earth

*Corresponding author. E-mail: nishio.katsuhisa@jaea.go.jp.
Fax: +81-29-282-5927.
†Josef Buchmann-Professor Laureatus.

elements.[7–10]

2. Experimental Methods

2.1. Measurement of fission cross sections. Measurement of the fission cross section was performed by using ^{30}Si beams supplied by the JAEA tandem accelerator facility in Tokai. The typical ^{30}Si-beam current was 1.0–2.5 pnA, and the beam energies were changed in the range from 140 MeV to 183 MeV to measure the excitation functions of the cross sections. The uranium target of 360 μg/cm^2 was made by electro-deposition on a Be-foil of 1.67 mg/cm^2 thickness, and the uranium layer was coated by a 0.84 μm aluminum foil. The target plane was tilted at 30° to the beam axis with the Be-foil facing the downstream of the beam, and the aluminum foil was facing fission fragment detectors described below.

Fission fragments were measured in singles mode by using ΔE-E detectors consisting of a gridded ionization detector and a silicon surface barrier detectors. The detectors were all mounted in single aluminum container. After passing through the 0.9 μm Mylar foil to shield the gas, fission fragments run through the 20 Torr isobutane gas layer with the distance 45 mm to give the ΔE signal, then implanted into the 300 mm^2 silicon detector to give the residual energy (E). In the container, three Si detectors were mounted at angles of 90°, 120°, and 150° relative to the beam direction to measure the angular distribution of the fission fragments. The grid and anode of the ΔE detector covered three directions. The solid angle to each direction was determined by the entrance Mylar window and was set at 2.13 msr. Another silicon surface barrier detector was placed at angle 45° relative to the beam direction to determine the absolute value of the fission cross sections. The solid angle was 1.08 msr.

Figure 1 shows examples of ΔE-E spectra obtained at two different energies of $E_{c.m.}$ = 150.0 MeV and 130.0 MeV at the middle layer of the target. The fission events can be distinguished from the elastic or quasi-elastic particles and other light particles.

For each beam energy, the differential fission cross section for three center-of-mass angles θ, $d\sigma/d\Omega(\theta)$, were fitted with a function describing the angular distribution of fission fragments $W(\theta)$ (Reference 11) as is explained in Reference 7. By integrating the fitted curve $W(\theta)$ over the solid angle, we obtained the fission cross section for each energy.

2.2. Measurement of evaporation residue cross sections. Measurement of the evaporation residue cross sections was performed using the velocity filter SHIP at the linear accelera-
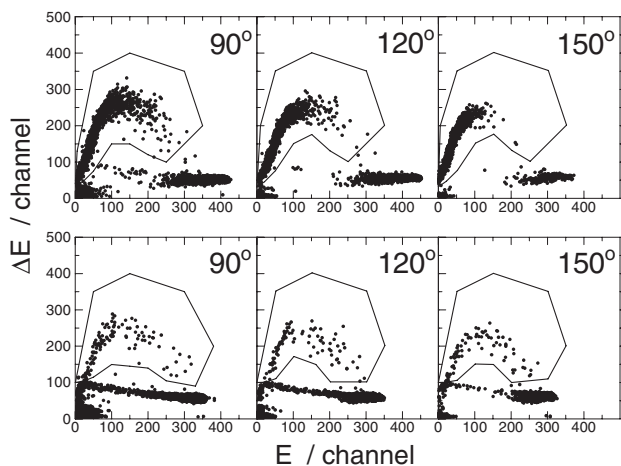
Figure 1. Detected particles on the two dimensional map on E and ΔE. The upper and lower panels show the data for the reaction energy $E_{c.m.}$ = 150.0 MeV and 130.0 MeV at the middle of the target, respectively. Spectra measured at angles of 90°, 120°, and 150° in laboratory frame are shown. Region for the fission events are enclosed by solid curves.

tor UNILAC of GSI in Darmstadt. The typical intensity of the ^{30}Si^{6+} beams was 0.7–1.0 pμA. The beam has time structure of 5.0 ms in width and 50 Hz in frequency. The detailed information for the experiment is published in Reference 6, so that the brief description on the experimental method is given here.

The experimental setup consists of a rotating target wheel, the velocity filter SHIP, and the detector system at the focal plane. Detailed descriptions can be found in References 1 and 12–15.

The uranium targets were prepared by evaporating the ^{238}UF$_4$ material on a 45 μg/cm^2 carbon backing with a thickness of 375–404 μg/cm^2. The uranium layer were coated with a 15 μg/cm^2 thick carbon.

The transmission effciency of SHIP was determined by using a Monte Carlo calculation, and we obtained 10% for the probability of ERs being transmitted and focused at the focal plane.

In the focal plane of the SHIP, ERs and their subsequent α decay and/or spontaneous fission (sf) are detected by a position sensitive 16-strip Si PIPS detector. Escaping α particles or fission fragment are detected by a 'box detector' which covers an area of 85% of the backward hemisphere. The energy resolution for fully stopped α's was typically 25 keV (FWHM) for the 8415 keV α particles from ^{252}No. For escaped α particles detected in coincidence with signals from the box detector, the resolution was determined to be 70 keV.

A timing detector is located in front of the silicon detector array to perform the time-of-flight measurement of the transmitted particles. Together with signals from the silicon detector, it was used for distinguishing implanted signals from radioactive decay events. The timing detector was moved out during some of the irradiations at the beginning of the experiment. In this case the radioactive decays were detected during the 15.0 ms beam off periods.

The spontaneous fission (sf) events are measured by detecting high energy deposition in the silicon detectors. The calibration was performed with α particles from external sources. The total kinetic energy (TKE) of sf events was obtained by summing the energies from the stop and the box detectors. Energy calibration of the TKE was performed by referring to the known TKE of 195 MeV of ^{252}No (Reference 16) produced in the reaction ^{48}Ca + ^{206}Pb. The pulse height deficit and the energy loss in the entrance windows of stop and box detectors were determined from the difference between the literature value and the measured energy based on the α-lines calibration. In this calibration run, we found a strong dependence of the measured fission fragment energies on the implantation depth of ERs, which was regulated by changing the thickness of Mylar degrader foils in front of the Si detectors. The results are shown in Figure 2. The implantation depth was calculated by the SRIM code.[17] Taking into account the calculated implantation depth of 1.6 μm for ERs produced in ^{30}Si + ^{238}U, 55 MeV should be added to the measured values to get the correct value of TKE.

Behind the focal-plane detector we mounted a clover detector consisting of four Ge crystals (50 mmϕ × 70 mm length). It was used to measure coincident γ- or X-rays accompanied by spontaneous fissions, whose signals were served as strong evidence for the occurrence of sf.

The detection of correlated events is primarily based on agreement of the measured positions between implanted ERs and subsequent α decays or sf.

3. Experimental Results and Discussions

3.1. Fission cross section for ^{30}Si + ^{238}U. Experimental results of the fission cross sections for ^{30}Si + ^{238}U are shown in the upper part of Figure 3. The fission fragments should originate from quasifission and compound nucleus fission, so that
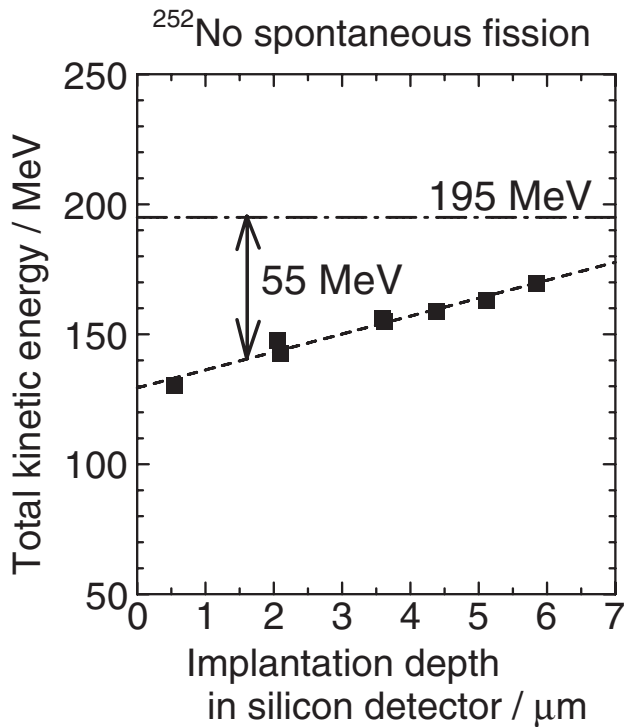
Figure 2. Sum of the energy of two fragments recorded by the stop and box detectors for the spontaneous fission of ^{252}No, which shows the dependence on the implanted depth in the stop detector. The literature value TKE = 195 MeV for ^{252}No is indicated. Implantation depth of ERs for ^{30}Si + ^{238}U is also shown, and the correction energy of 55 MeV is obtained.

Figure 3. (Upper part) Fission cross sections of the reaction ^{30}Si + ^{238}U as function of center-of-mass energy $E_{c.m.}$ and excitation energy E^*. The data are compared with coupled channels calculation (full line) and the one dimensional fusion model (dashed line). (Lower part) Results of the evaporation residue cross sections. Calculation of the statistical model by using the code HIVAP[34] are shown, where the partial cross sections from the CCDEGEN code[18] was used as input. At $E_{c.m.} = 133.0$ and 144.0 MeV three events were measured in each case for the 4n (diamond) and 5n (circle) evaporation channel, respectively, and one event in each case was tentatively assigned to the 3n (open triangle) and 6n (open square) channel, respectively. The two extreme touching configurations, polar and equatorial collisions are shown at the top. The arrows indicate the corresponding Coulomb barrier heights.
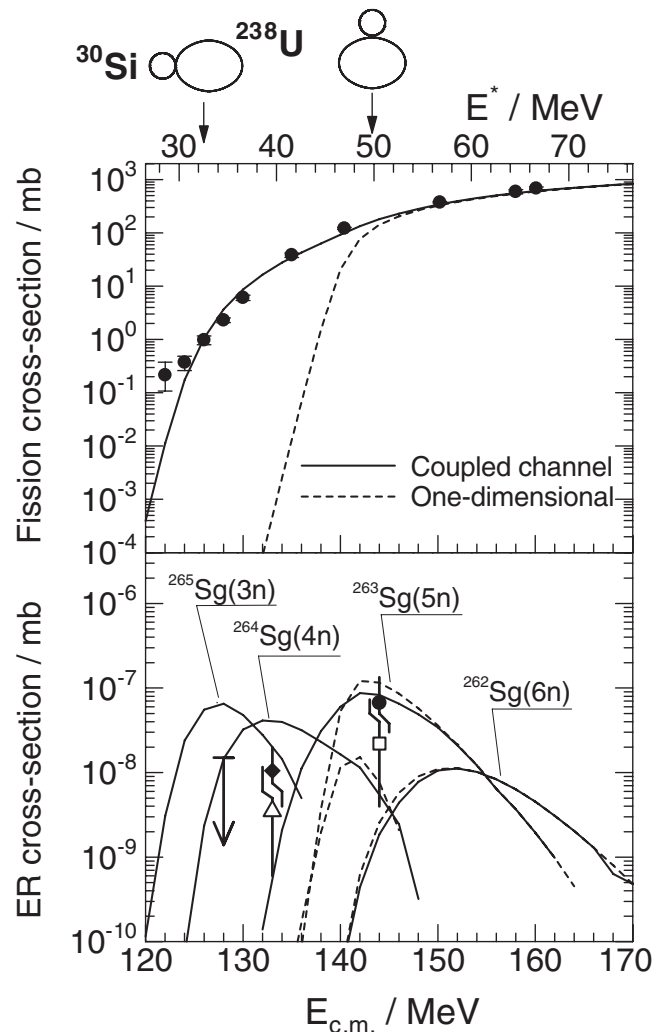
the cross section represents the sum of both origins. The data are compared with the calculated capture cross section using the coupled channel code CCDEGEN[18] which is a modification of the code CCFULL.[19] In the calculation static deformation of the target nucleus ^{238}U with the deformation parameters of $\beta_2 = 0.275$ and $\beta_4 = 0.05$ is taken into account.[5,20] The nuclear potential was approximated with the same parameters as in the case of the previously studied reaction ^{16}O + ^{238}U → ^{254}Fm*.[5] Also considered was the channel coupling to the 3$^-$ state at 0.73 MeV in ^{238}U and to the 2$^+$ state at 2.235 MeV in ^{30}Si.[21] We also show in Figure 3 the results from the CCDEGEN code by ignoring deformation of ^{238}U and couplings to the vibrational states in the nuclei (one dimensional model). The corresponding Coulomb barrier height is 139.7 MeV, which is almost equal to the Bass barrier energy 141.4 MeV.[22]

The coupled channel calculation reproduces well the experimental data points for the reaction ^{30}Si + ^{238}U. On the other hand the one dimensional model cannot describe the data below the energy $E_{c.m.} = 140$ MeV.

3.2. Produced evaporation residues and their decay properties. For the production of evaporation residues in the ^{30}Si + ^{238}U, we used three different center-of-mass energies $E_{c.m.}$ (excitation energies E^*) of 144.4 (50.6), 133.0 (39.6), and 128.0 (34.5) in MeV at the half thickness of the target layer. The accumulated beam doses were 1.8×10^{18}, 4.0×10^{18}, and 1.7×10^{18} particles, respectively.

At the highest energy of $E_{c.m.} = 144.5$ MeV we expect the highest cross section for the well known isotope ^{263}Sg (References 23–28) produced in the 5n channel. In this energy we observed decay events as shown in the upper row on Figure 4, chronologically ordered from 1 to 4.
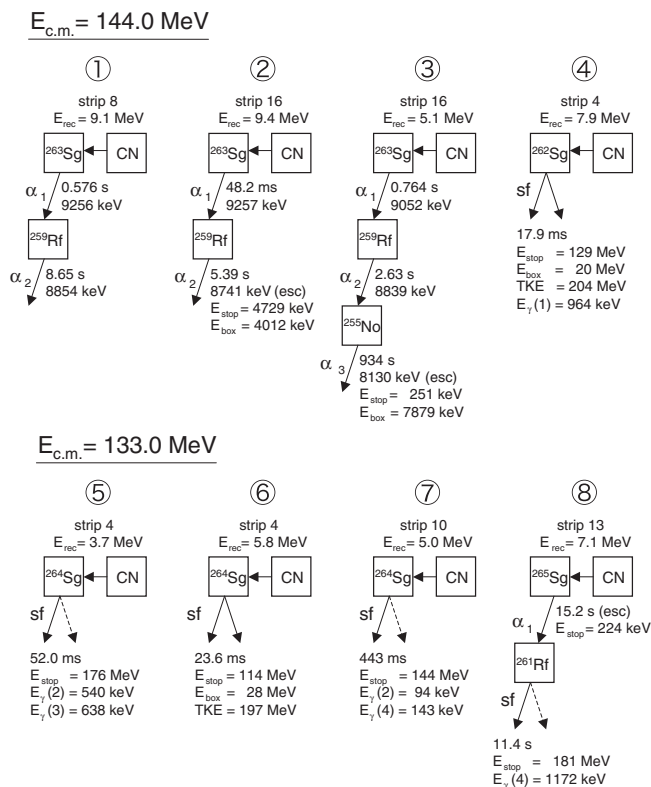
Subsequent to the implantation we measured at the same position of the detector within the position resolution two α decays in the case of event number 1 and 2, three α decays in the case of event number 3. Energies and half-lives agree well with the literature data for ^{263}Sg (see references given before).

The 9.06 and 9.25 MeV lines were reported for the α decay of ^{263}Sg both in the direct production in a fusion reaction[23] and in the α decay from ^{271}Ds.[25–28] Two different lines should originate from two different levels in ^{263}Sg. In the case of the direct production in ^{18}O + ^{249}Cf,[23] the 9.05 MeV line is dominated. In the decay chains of ^{271}Ds, the 9.25 MeV α particles are observed almost exclusively.[25–28] From the 22 events in References 25–28, the majority of 20 decays belongs to the higher energy of 9.25 MeV and only 2 have the energy of 9.06 MeV. The mean half-lives for two groups are determined to be $(0.56^{+0.16}_{-0.10})$ s and $(0.56^{+1.02}_{-0.22})$ s, respectively.

In the present experiment we observed two α decays at 9.25 MeV and one at 9.05 MeV. The measured lifetimes given in Figure 4 are in good agreement with the literature data. The present intensity ratio of two to one for the energetically different α particles may indicate losses of the shorter-lived higher-energy α particles in the He-jet experiment.[23] The cross section for the production of three ^{263}Sg nuclei in our experiment at $E_{c.m.} = 144.4$ MeV is (67^{+67}_{-37}) pb.

$E_{c.m.}$ = 144.0 MeV

① ② ③ ④

strip 8
E_{rec} = 9.1 MeV
²⁶³Sg ← CN
α_1 0.576 s
9256 keV
²⁵⁹Rf
α_2 8.65 s
8854 keV

strip 16
E_{rec} = 9.4 MeV
²⁶³Sg ← CN
α_1 48.2 ms
9257 keV
²⁵⁹Rf
α_2 5.39 s
8741 keV (esc)
E_{stop} = 4729 keV
E_{box} = 4012 keV

strip 16
E_{rec} = 5.1 MeV
²⁶³Sg ← CN
α_1 0.764 s
9052 keV
²⁵⁹Rf
α_2 2.63 s
8839 keV
²⁵⁵No
α_3 934 s
8130 keV (esc)
E_{stop} = 251 keV
E_{box} = 7879 keV

strip 4
E_{rec} = 7.9 MeV
²⁶²Sg ← CN
sf
17.9 ms
E_{stop} = 129 MeV
E_{box} = 20 MeV
TKE = 204 MeV
$E_\gamma(1)$ = 964 keV

$E_{c.m.}$ = 133.0 MeV

⑤ ⑥ ⑦ ⑧

strip 4
E_{rec} = 3.7 MeV
²⁶⁴Sg ← CN
sf
52.0 ms
E_{stop} = 176 MeV
$E_\gamma(2)$ = 540 keV
$E_\gamma(3)$ = 638 keV

strip 4
E_{rec} = 5.8 MeV
²⁶⁴Sg ← CN
sf
23.6 ms
E_{stop} = 114 MeV
E_{box} = 28 MeV
TKE = 197 MeV

strip 10
E_{rec} = 5.0 MeV
²⁶⁴Sg ← CN
sf
443 ms
E_{stop} = 144 MeV
$E_\gamma(2)$ = 94 keV
$E_\gamma(4)$ = 143 keV

strip 13
E_{rec} = 7.1 MeV
²⁶⁵Sg ← CN
α_1 15.2 s (esc)
E_{stop} = 224 keV
²⁶¹Rf
sf
11.4 s
E_{stop} = 181 MeV
$E_\gamma(4)$ = 1172 keV

Figure 4: Decay events obtained from the reaction ^{30}Si + ^{238}U → ^{268}Sg* at $E_{c.m.}$ = 144.0 MeV (upper row) and at $E_{c.m.}$ = 133.0 MeV (lower row). In the case of α decay or spontaneous fission (sf) the energies measured in the stop and box detectors are given. The total kinetic energy (TKE) of sf is given, when both fission fragments were detected. Also given are the energies of γ rays coincident with sf measured in one or more of the four crystals of the Ge clover detector. The number in brackets gives the crystal number of the four fold Ge clover detector.

At the highest beam energy we also observed one sf event with lifetime of 17.9 ms ($T_{1/2}$ = (12.4$^{+56}_{-6}$) ms), number 4 in Figure 4. The sf event was in coincidence with a γ ray at 964 keV in one of the crystals of the clover detector. Two fragments were measured in coincidence with the stop and box detector, and we obtained 204 MeV as TKE after correcting for the pulse height deficit of 55 MeV. The cross section for the sf event was (22$^{+51}_{-18}$) pb. We tentatively assign this sf event to the isotope ^{262}Sg produced by evaporation of six neutrons. The measured TKE of 204 MeV agrees reasonably with the value of 210 MeV based on the empirical Viola formula[29] for ^{262}Sg as shown in Figure 5.

At the lower beam energy of $E_{c.m.}$ = 133.0 MeV, we observed four sf events as numbered from 5 to 8 in Figure 4. In the case of event numbers 5, 7, and 8, coincident γ signals from the clover detector were observed. In the case of event number 6, both fission fragments were detected in the stop and box detector, and this event occurred during the beam-off period. From the sum of the two fragment energies, we obtained a TKE of 197 MeV after correcting for the pulse height deficit.

The lifetimes of the sf events number 5 to 7 are similar to each other and relatively short. We determined a half-life of (120$^{+126}_{-44}$) ms. These events were produced at an excitation energy of 40 MeV, 11 MeV less than the value for the production of ^{263}Sg. We assign these three sf events to the isotope ^{264}Sg. The TKE of 197 MeV for event number 6 has reasonable agreement with 210 MeV calculated with the Viola formula for ^{264}Sg (Reference 29) as shown in Figure 5.

In Figure 6, the partial half-lives for the Sg isotopes are shown. The data for ^{258,260,262}Sg are taken from References 31 and 30. Recent data for ^{266}Sg are taken from Reference 32. We also show in Figure 6 the theoretical calculation of the sf par-
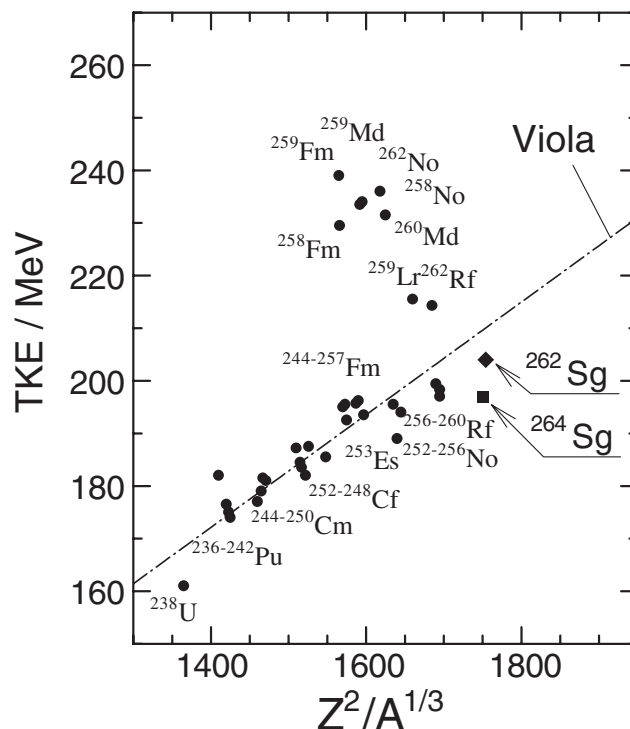
Figure 5: Total kinetic energies of the spontaneously fissioning nuclei are shown as a function of $Z^2/A^{1/3}$. The present data for ^{262}Sg and ^{264}Sg fissions are shown. Dash-dotted line is the Viola formula.[29]
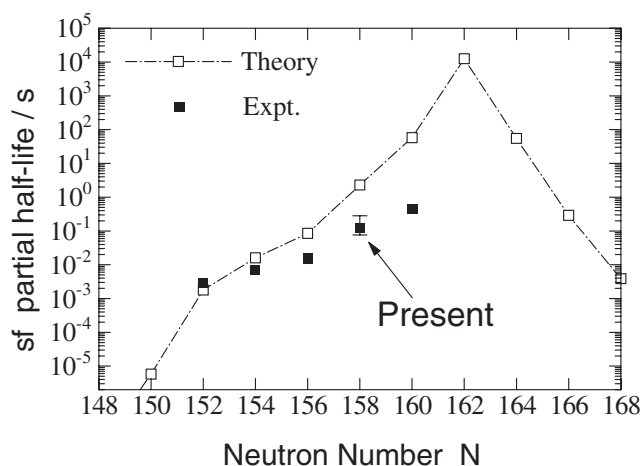
Figure 6: Partial half-lives for spontaneous fission of the Sg isotopes (solid squares) are compared with the theoretical calculation[33] (open squares connected by the dash-dotted lines). The present data for ^{264}Sg is indicated.

tial half-life.[33] The calculated half-life for ^{264}Sg is 2.3 s, which is about factor ten longer than our data.

The production cross section for the three sf events assigned to ^{264}Sg is (10$^{+10}_{-6}$) pb.

Before the 11.4 s of the sf event of number 8, we observed an escaped α particle with 224 keV signal. Then the ER candidate prior to the sf event and escaped α particle was detected at 15.2 s before the α event. However, due to the appearance of one ER-like event every 10 s on the average, the value of 15.2 s represents only a lower limit for the lifetime. We tentatively assign this chain originating from the escaped α decay of ^{265}Sg followed by spontaneous fission of ^{261}Rf as is discussed in Reference 6. The production cross section of this decay is (3.5$^{+8.1}_{-2.9}$) pb.

At the lowest beam energy of $E_{c.m.}$ = 128.0 MeV no decay events were measured. We determined an upper cross-section limit of 15 pb at 68% confidence level (one event corresponds to 8.2 pb).

Measurement of Evaporation Residue and Fission Cross Sections

J. Nucl. Radiochem. Sci., Vol. 8, No. 2, 2007 **77**

3.3. Discussion of the production cross sections. Experimental results for the ER cross sections in the reaction of ^{30}Si + ^{238}U → ^{268}Sg* are compared with model calculations as shown in the lower part of Figure 3. Using the two different models for the capture cross section (entrance channel), i.e., the coupled channel calculation and one dimensional model, the ER cross sections are calculated with the statistical model code HIVAP.[34]

The measured ER cross section for the 5n channel, ^{263}Sg, at $E_{c.m.}$ = 144.0 MeV agrees well with both calculations, the coupled channel calculation and the one dimensional calculation.

At the lower energy $E_{c.m.}$ = 133.0 MeV the large enhancement of the 4n ER cross section compared to the one dimensional model confirms the validity of taking into account the properties of colliding nucleus. Especially the enhancement is caused by the lowering of the Coulomb barrier height for collisions at the polar sides of ^{238}U. However, the experimental 4n cross section (10 pb) is about factor of 4 smaller than the calculated cross section (40 pb). This suggests the competition between fusion and quasifission after system is captured inside the Coulomb barrier. Also at the lowest energy $E_{c.m.}$ = 128.0 MeV the measured upper limit of the cross section of 15 pb (3n + 5n channel) is about a factor 5 less than the calculation, suggesting the presence of quasifission.

Finally we compare the two extreme reactions mentioned before, namely the very asymmetric system ^{16}O + ^{238}U (Reference 5) which has fusion probability independent of orientation and the heaviest systems studied so far using ^{48}Ca projectiles,[3,4] with the reaction ^{30}Si + ^{238}U studied here. The reaction ^{30}Si + ^{238}U shows an intermediate behavior. We observed a measurable fusion cross section at subbarrier energies, where a contact is limited to polar collisions, but indicated a competition between quasifission and complete fusion. On the other hand, no suppression of the ER cross section was measured at the energy where contact of the projectile on the equatorial side of ^{238}U is possible, suggesting that the fusion starting from the compact configuration results in higher fusion probability.

References

(1) S. Hofmann and G. Münzenberg, Rev. Mod. Phys. **72**, 733 (2000).

(2) K. Morita, K. Morimoto, D. Kaji, T. Akimura, S. Goto, H. Haba, E. Ideguchi, R. Kanungo, K. Kaori, H. Koura, H. Kudo, T. Ohnishi, A. Ozawa, T. Suda, K. Sueki, H. Xu, T. Yamaguchi, A. Yoneda, A. Yoshida, and Y. Zhao, J. Phys. Soc. Jpn. **73**, 1738 (2004).

(3) Yu. Ts. Oganessian, V. K. Utyonkov, Yu. V. Lobanov, F. Sh. Abdullin, A. N. Polyakov, I. V. Shirokovsky, Yu. S. Tsyganov, G. G. Gulbekian, S. L. Bogomolov, B. N. Gikal, A. N. Mezentsev, S. Iliev, V. G. Subbotin, A. M. Sukhov, A. A. Voinov, G. V. Buklanov, K. Subotic, V. I. Zagrebaev, M. G. Itkis, J. B. Patin, K. J. Moody, J. F. Wild, M. A. Stoyer, N. J. Stoyer, D. A. Shaughnessy, J. M. Kenneally, and R. W. Lougheed, Phys. Rev. C **69**, 054607 (2004).

(4) Yu. Ts. Oganessian, V. K. Utyonkov, Yu. V. Lobanov, F. Sh. Abdullin, A. N. Polyakov, I. V. Shirokovsky, Yu. S. Tsyganov, G. G. Gulbekian, S. L. Bogomolov, B. N. Gikal, A. N. Mezentsev, S. Iliev, V. G. Subbotin, A. M. Sukhov, A. A. Voinov, G. V. Buklanov, K. Subotic, V. I. Zagrebaev, M. G. Itkis, J. B. Patin, K. J. Moody, J. F. Wild, M. A. Stoyer, N. J. Stoyer, D. A. Shaughnessy, J. M. Kenneally, P. A. Wilk, R. W. Lougheed, R. I. Il'kaev, and S. P. Vesnovskii, Phys. Rev. C **70**, 064609 (2004).

(5) K. Nishio, H. Ikezoe, Y. Nagame, M. Asai, K. Tsukada, S. Mitsuoka, K. Tsuruta, K. Satou, C. J. Lin, and T. Ohsawa, Phys. Rev. Lett. **93**, 162701 (2004).

(6) K. Nishio, S. Hofmann, F. P. Heßberger, D. Ackermann, S. Antalic, V. F. Comas, Z. Gan, S. Heinz, J. A. Heredia, H. Ikezoe, J. Khuyagbaatar, B. Kindler, I. Kojouharov, P. Kuusiniemi, B. Lommel, R. Mann, M. Mazzocco, S. Mitsuoka, Y. Nagame, T. Ohtsuki, A. G. Popeko, S. Saro, H. J. Schött, B. Sulignano, A. Svirikhin, K. Tsukada, K. Tsuruta, and A. V. Yeremin, Eur. Phys. J. A **29**, 281 (2006).

(7) K. Nishio, H. Ikezoe, S. Mitsuoka, and J. Lu, Phys. Rev. C **62**, 014602 (2000).

(8) S. Mitsuoka, H. Ikezoe, K. Nishio, and J. Lu, Phys. Rev. C **62**, 054603 (2000).

(9) K. Nishio, H. Ikezoe, S. Mitsuoka, K. Satou, and S. C. Jeong, Phys. Rev. C **63**, 044610 (2001).

(10) S. Mitsuoka, H. Ikezoe, K. Nishio, K. Satou, and J. Lu, Phys. Rev. C **65**, 054608 (2002).

(11) B. B. Back, R. R. Betts, J. E. Gindler, B. D. Wilkins, S. Saini, M. B. Tsang, C. K. Gelbke, W. G. Lynch, M. A. McMahan, and P. A. Baisden, Phys. Rev. C **32**, 195 (1985).

(12) G. Münzenberg, W. Faust, S. Hofmann, P. Armbruster, K. Güttner, and H. Ewald, Nucl. Instrum. Methods **161**, 65 (1979).

(13) S. Hofmann, W. Faust, G. Münzenberg, W. Reisdorf, P. Armbruster, K. Güttner, and H. Ewald, Z. Phys. A **291**, 53 (1979).

(14) H. Folger, F. P. Heßberger, S. Hofmann, J. Klemm, G. Münzenberg, V. Ninov, W. Thalheimer, and P. Armbruster, Nucl. Instrum. Methods Phys. Res. A **362**, 64 (1995).

(15) B. Lommel, D. Gembalies-Datz, W. Hartmann, S. Hofmann, B. Kindler, J. Klemm, J. Kojouharov, J. Steiner, Nucl. Instrum. Methods Phys. Res. A **480**, 16 (2002).

(16) E. K. Hulet, Phys. At. Nucl. **57**, 1099 (1994).

(17) http://www.srim.org/.

(18) K. Hagino (unpublished).

(19) K. Hagino, N. Rowley, and A. T. Kruppa, Comput. Phys. Comm. **123**, 143 (1999).

(20) D. J. Hinde, M. Dasgupta, J. R. Leigh, J. P. Lestone, J. C. Mein, C. R. Morton, J. O. Newton, and H. Timmers, Phys. Rev. Lett. **74**, 1295 (1995).

(21) R. B. Firestone and V. S. Shirley, *Table of Isotopes, Eighth Edition*, John Wiley & Sons, Inc., New York (1996).

(22) R. Bass, *Nuclear Reactions with Heavy Ions*, Springer-Verlag, Berlin (1980).

(23) A. Ghiorso, J. M. Nitschke, J. R. Alonso, C. T. Alonso, M. Nurmia, G. T. Seaborg, E. K. Hulet, and R. W. Lougheed, Phys. Rev. Lett. **33**, 1490 (1974).

(24) S. Hofmann, Rep. Prog. Phys. **61**, 639 (1998).

(25) S. Hofmann, J. Nucl. Radiochem. Sci. **4**, R1 (2003).

(26) T. N. Ginter, K. E. Gregorich, W. Loveland, D. M. Lee, U. W. Kirbach, R. Sudowe, C. M. Folden, III, J. B. Patin, N. Seward, P. A. Wilk, P. M. Zielinski, K. Aleklett, R. Eichler, H. Nitsche, and D. C. Hoffman, Phys. Rev. C **67**, 064609 (2003).

(27) K. Morita, K. Morimoto, D. Kaji, H. Haba, E. Ideguchi, R. Kanungo, K. Katori, H. Koura, H. Kudo, T. Ohnishi, A. Ozawa, T. Suda, K. Sueki, I. Tanihata, H. Xu, A.V. Yeremin, A. Yoneda, A. Yoshida, Y.-L. Zhao, and T. Zheng, Eur. Phys. J. A **21**, 257 (2004).

(28) C. M. Folden III, K. E. Gregorich, Ch. E. Düllmann, H. Mahmud, G. K. Pang, J. M. Schwantes, R. Sudowe, P. M. Zielinski, H. Nitsche, and D. C. Hoffman, Phys. Rev. Lett. **93**, 212702 (2004).

(29) V. E. Viola, Jr., Nucl. Data Sect. A **1**, 391 (1966).

(30) S. Hofmann, F. P. Heßberger, D. Ackermann, S. Antalic, P. Cagarda, S. Cwiok, B. Kindler, J. Kojouharova, B. Lommel, R. Mann, G. Münzenberg, A. G. Popeko, S. Saro, H. J. Schött, and A. V. Yeremin, Eur. Phys. J. A **10**, 5 (2001).

(31) M. Leino and F. P. Heßberger, Ann. Rev. Nucl. Part. Sci. **54**, 175 (2004).

(32) J. Dvorak, W. Brüchle, M. Chelnokov, R. Dressler, Ch. E. Düllmann, K. Eberhardt, V. Gorshkov, E. Jäger, R. Krücken, A. Kuznetsov, Y. Nagame, F. Nebel, Z. Novackova, Z. Qin, M. Schädel, B. Schausten, E. Schimpf, A. Semchenkov, P. Thörle, A Türler, M. Wegrzecki, B. Wierczinski, A. Yakushev, and A. Yeremin, Phys. Rev. Lett. **97**, 242501 (2006).

(33) R. Smolańczuk, J. Skalski, and A. Sobiczewski, Phys. Rev. C **52**, 1871 (1995).

(34) W. Reisdorf and M. Schädel, Z. Phys. A **343**, 47 (1992).